Environmental Engineering and Management Journal November 2014, Vol.13, No. 11, 2817-2824
http://omicron.ch.tuiasi.ro/EEMJ/

"Gheorghe Asachi" Technical University of Iasi, Romania

MODELING AND VIBRATION ANALYSIS OF LIMESCALE DEPOSITION IN GEOTHERMAL PIPES

Dénes Kocsis*

University of Debrecen, Department of Chemical and Environmental Engineering, 2-4 Ótemető Street, Debrecen, HU-4028, Hungary

Abstract

Failures of geothermal system pipes are often caused by limescale buildup on the walls of the pipes. The primary aim of this work is to investigate the influence of the scale formed on the walls of the pipes on the vibration parameters and natural frequencies of pipelines. To this end, the different phases of deposition are artificially simulated in the model experiments. In the different states, vibration tests are preformed to evaluate the status of the pipe section and the rate of deposition by a nondestructive technique. The experimental system is also analyzed by the finite element method (FEM), and the obtained results are compared.

Key words: finite elements, limescale buildup, natural frequencies, piping vibration

Received: February, 2014; Revised final: October, 2014; Accepted: October, 2014

1. Introduction

Pipelines are important elements of geothermal systems, the failures of which cause significant financial and environmental damage in many cases. A remarkable part of the total failure can be traced back to damage or failure of pipes (Drozyner, 2011); therefore, this topic deserves special attention, as is indicated by the large number of related publications.

Vibration-based diagnostic tests are often used to assess the failure or the status of materials and structures. Impulse excitation of vibration (IEV) is a suitable method for assessments of the condition and identification of the errors. Raggio et al. (2010) performed error analysis of the IEV measurement in steel samples. Kajiwara and Hosoya (2011) also conducted tests measuring IEV; however, the excitation was not implemented by an impulse hammer but using a laser ablation, which enabled the examination of high frequency elements in the region of tens of kilohertz. This approach can be a suitable technique in the high frequency range because it does not require the measurement of the input force (Hosoya et al., 2012). Another widely applied method based on time-of-flight (ToF) was used by Lee et al. (2011) to assess a wall-thinned pipe.

Determination of the natural frequencies during the examination of pipes provides the basis of the tests in many cases, such as in the works of Wang and Redekop (2011) and Saeed et al. (2013). The latter authors performed three-dimensional (3D) fluid-structure modeling and vibration analysis for fault diagnosis. Li et al. (2014) examined pipes conveying fluid by the transfer matrix method and determined their natural frequencies and frequency responses.

The investigation performed by Mattheis et al. (2000) was based on the fact that changes in system stiffness are reflected in the changes in the experimentally defined natural frequencies. Our investigation is performed along this assumption, and the scaling on the internal wall of the pipes, as one of the most typical problems of geothermal piping

* Author to whom all correspondence should be addressed: E-mail: kocsis.denes@eng.unideb.hu; Phone: +36 52 415-155; Fax: +36 (52) 418-643

systems, needs to be modeled. For this purpose, the characteristic parameters of a pipe element in laboratory conditions are investigated by the vibration diagnostic technique. In the literature, the results of similar tests can be determined for the examination of the properties of piping systems, such as in the work of Semke et al. (2006), where vibration diagnostic tests were conducted in model experiments on bolted flange piping systems.

In our investigation, the measurements are performed on a stainless steel pipe. The measurement sequence is designed such that after performing the baseline measurements, concrete layers of varying thickness are formed on the inner surface of the pipe, and the measurements are performed during the different in-between states.

Concrete is selected for modeling the amount of scale formed on the pipe's inner wall, because from the perspective of feasibility, it appears to be the most advantageous, and it has similar mechanical properties to scale. Note that the density of both materials varies between relatively high thresholds.

2. Materials and methods

The experiments are performed on a stainless steel pipe with external diameters of 89 mm and wall thicknesses of 2 mm. This type of pipe is chosen for the examination because geothermal pipe sections of the same size are regularly exposed to failure due to scaling in several Hungarian cities (Zalaegerszeg, Kistelek).

The total length of the examined pipe is 1115 mm, and the measurements are executed on a metalworking lathe, where the pipe has been supported by two steady rests. For this support, longitudinally cut steel pipe parts are used along with 3-mm-thick rubber pieces placed beneath them; these elements are used to support the pipe. The pipe length between the steady rests is 800 mm. The scheme of the experimental layout is shown in Fig. 1.

For the vibration test, two pieces of triaxial accelerometers are glued to the pipe with the arrangement shown in Fig. 1. One sensor is placed in the middle of the 800-mm-long section (accelerometer 1), while the other (accelerometer 2) is placed close to a steady rest (350 mm distance from the accelerometer 1). The fixed pipe can be seen in Fig. 2 on which tests are performed with impulse excitation of vibration from various directions and at multiple locations.

The IEV is executed both by hammer and dropped golf ball (weight of golf ball: 45.81 g) from defined height (0.5 m). In addition, tests are performed in which 50 Hz excitation is applied from the front direction under the centrally placed sensor (accelerometer 1) by a frequency generator. After the baseline measurement, scaling on the inner surface of the pipe is simulated by concrete layers. This simulation is performed in three steps, and in each step, a new concrete layer is formed on the inner surface.

The mixed concrete is poured into the pipe, which is rotated for 1 hour in a lathe afterwards. Next, the pipe is taken off from the lathe and left for curing. For the workability of the concrete, end plugs designed for this purpose are placed, which are still in the tubes during the measurements. The inner diameter changes for the three concrete layers and the applied rotational speed are presented in Table 1.

In addition to the ease of modeling the scale layer, using concrete has the advantage of exhibiting similar characteristics to the scale layer in many cases. The ranges of the density values of the two materials used for natural frequency calculations are partially overlapping. The concrete layer forms an irregular circular inner diameter, which can also be observed for scaling processes in many cases. The rotational speed is increased during the experiments to obtain a smoother concrete surface. Fig. 3 shows a pipe during the rotation on the lathe and the result of the application of concrete level 1.

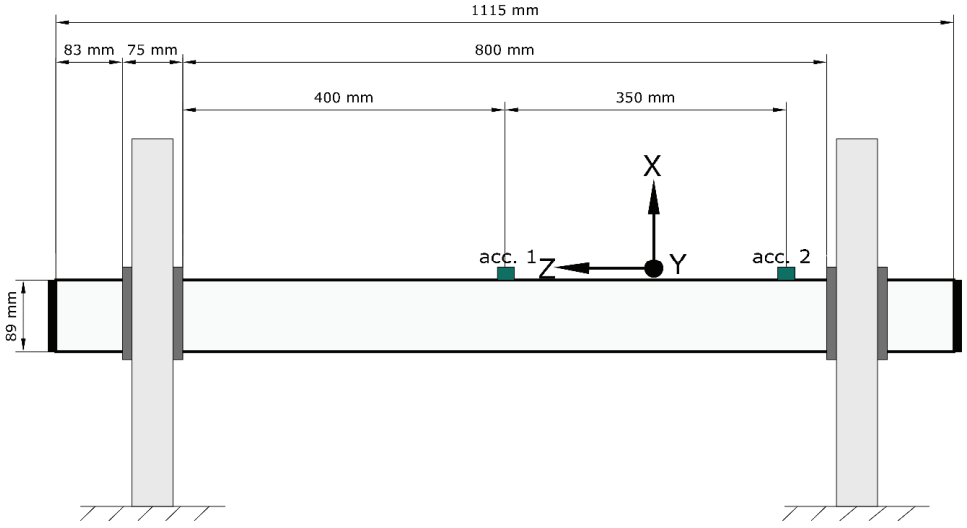

Fig. 1. Experimental layout

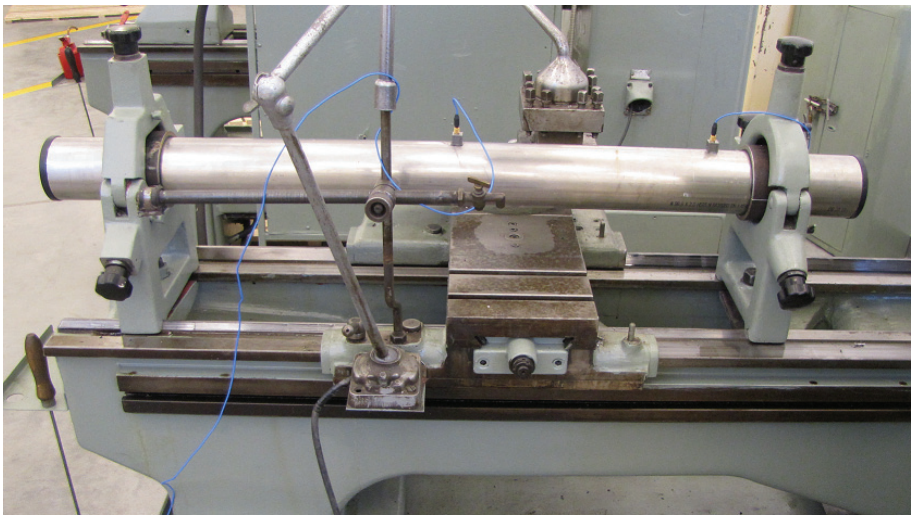

Fig. 2. The pipe position and the location of the glued accelerometers

Table 1. The decreasing inner diameter values as a result of the added concrete layers and the applied rotational speed

Phase of layer forming	*The approximately value of the new inner diameter [mm]*	*Rotational speed [1/min]*
Concrete level 1	65	75
Concrete level 2	50	150
Concrete level 3	40	240

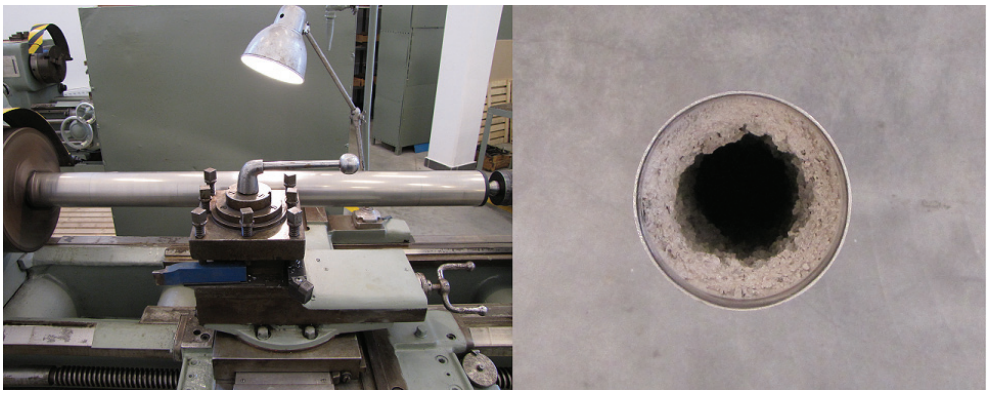

Fig. 3. The pipe during the rotation on the lathe and after the application of concrete level 1

3. Experimental

During the experiments, the measurements are performed on the section between the two steady rests. On this section, the piping span longitudinal natural frequencies deviate from the theoretical beam natural frequencies. The single span beam can longitudinally oscillate in different mode shapes, the natural frequencies (f_0) of which can be calculated using Eq. (1) (Bajcar et al., 2010; Wachel et al. 1990):

$$f_0 = \frac{\lambda}{2\pi l^2}\sqrt{\frac{EI}{m}} \tag{1}$$

where l is the length, E is the material's modulus of elasticity, I is the cross-sectional mass moment of inertia, m is mass per unit length of beam and λ is the dimensionless frequency factor, which depends on the piping configuration and on the number of the natural frequency. The value of the λ for the first natural frequency in the case of fixed-fixed piping configuration is 22.4 and in the case of simply supported piping configuration is 9.87 (Wachel et al., 1990). In addition to the longitudinal vibration, the circumferential vibration of the piping shell can also occur (Liu et al., 2005), which should be considered during our examinations. For the natural frequency calculation of these shell wall vibrations, Eq. (2) can be used (Bajcar et al., 2010; Wachel et al., 1990):

$$f_0 = \frac{\lambda_i}{2\pi R}\sqrt{\frac{E}{\rho(1-\nu^2)}} \tag{2}$$

where: R is the mean radius of pipe wall, ρ is the mass density of pipeline material, and ν is Poisson's ratio. λ_i is a dimensionless frequency factor, which

can be calculated using Eq.(3) (Bajcar et al., 2010; Wachel et al., 1990):

$$\lambda_i = \frac{t}{R\sqrt{12}} \frac{i(i^2-1)}{\sqrt{1+i^2}} \quad (3)$$

where: t is the pipe wall thickness, and I is the mode number.

Based on the measured values between the two steady rests section, examination of the piping configuration corresponding to the introduced system becomes possible. Furthermore, the investigation of what correction factor should be applied to match the measured and calculated values is also feasible. The vibration analysis is performed using the two triaxial sensors placed on the pipeline. For excitation, IEV is applied, which is performed in several places, from multiple directions, and over multiple repetitions.

The arrangement of the experiment with the two triaxial accelerometers can be appropriate for the examination of the vibration propagation speed, which is planned to be applied during in situ measurements. In this case, the distance between the sensors is relatively small compared to the vibration propagation speed; therefore, it cannot be analyzed by the devices used here.

A commercial software package is used for finite element modal analysis of the steel pipes (Racasan et al., 2011) partly filled with concrete. The system consists of parts made of four different materials: steel pipe, concrete layer on the inner surface of the pipe (with three various thickness), plastic stoppers closing the two end of the pipe, and the mechanical support with rubber pillows. Fig. 4 illustrates the assembly of discretized model of the system, and Fig. 5 shows the details of the mechanical support. 3D structural quadratic hexahedral elements are used for building up the bodies of the model. The contacts are set to be glued between parts touching each other. The material behavior is considered to be linear elastic, and the material properties are summarized in Table 2.

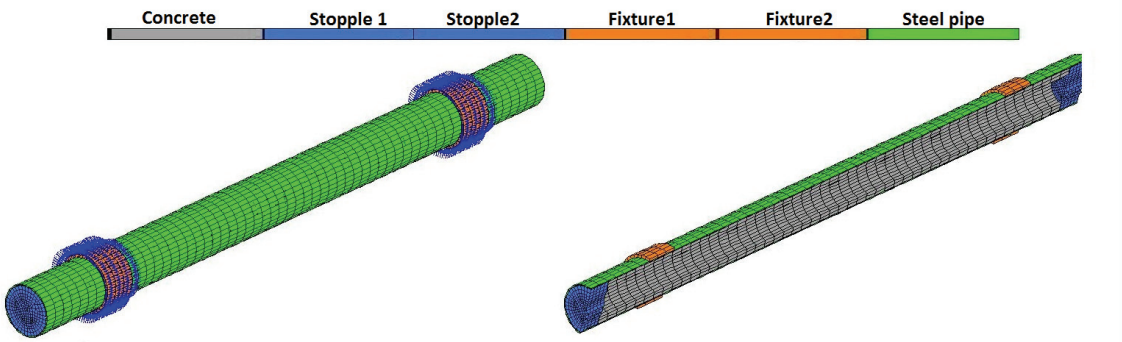

Fig. 4. The assembly of the system

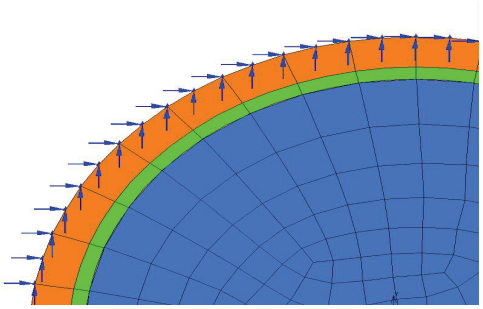

Fig. 5. Fixtures of the rubber support: nodes on outer surface are fixed, while the others are not

Table 2. Material properties used in the model calculations

Material	*Name of quantity*	*Value and unit*
Steel EN1.4541	Elastic modulus	200000 MPa
	Poisson's ratio	0.3
	Mass density	7900 kg/m^3
Rubber (support)	Elastic modulus	5.8 MPa
	Poisson's ratio	0.45
	Mass density	1000 kg/m^3
Concrete	Elastic modulus	22000 MPa
	Poisson's ratio	0.2
	Mass density	1600 kg/m^3
HDPE (material of stopples)	Elastic modulus	1035 MPa
	Poisson's ratio	0.45
	Mass density	1000 m^3

4. Results and discussion

In the experiment series, it is assumed that the pipeline's stiffness changes due to the concrete layer can be detected through the change of the natural frequencies. During the tests, consecutive measurements are performed with the same impulse excitation of vibration to eliminate errors. Fig. 6 represents the response for the same IEV of the pipe in the baseline state (Fig. 6a) and, subsequently, after the different concrete levels (Fig. 6b-6d). The figure series shows the measured acceleration values of the two accelerometer in the vertical (x) direction, perpendicular to the axis. The values in Fig. 6 all belong to the same type impulse excitation of vibration. The acceleration responses are observed to change significantly versus time based on the shapes and characteristics of the curves. On the basis of the figures, it can generally be declared that as the concrete layer on the pipe's inner wall becomes thicker, the amplitude responses for the same excitation becomes smaller, and that the number of the curve peaks in the lower frequency range decreases based on the shape and damping of the curves. The beginning of the obtained signal values versus time plots show the influence of the relatively high-frequency components, which are damped faster as time progresses, which are followed by the smaller frequency components, which dominate the signal in the later moments of time.

For the evaluation of the natural frequencies, the representative frequency spectra obtained by fast Fourier transform (FFT) provide opportunities. In Fig. 7, the FFT spectrums for the previously highlighted same IEV can be observed in the pipe's baseline and after different concrete levels.

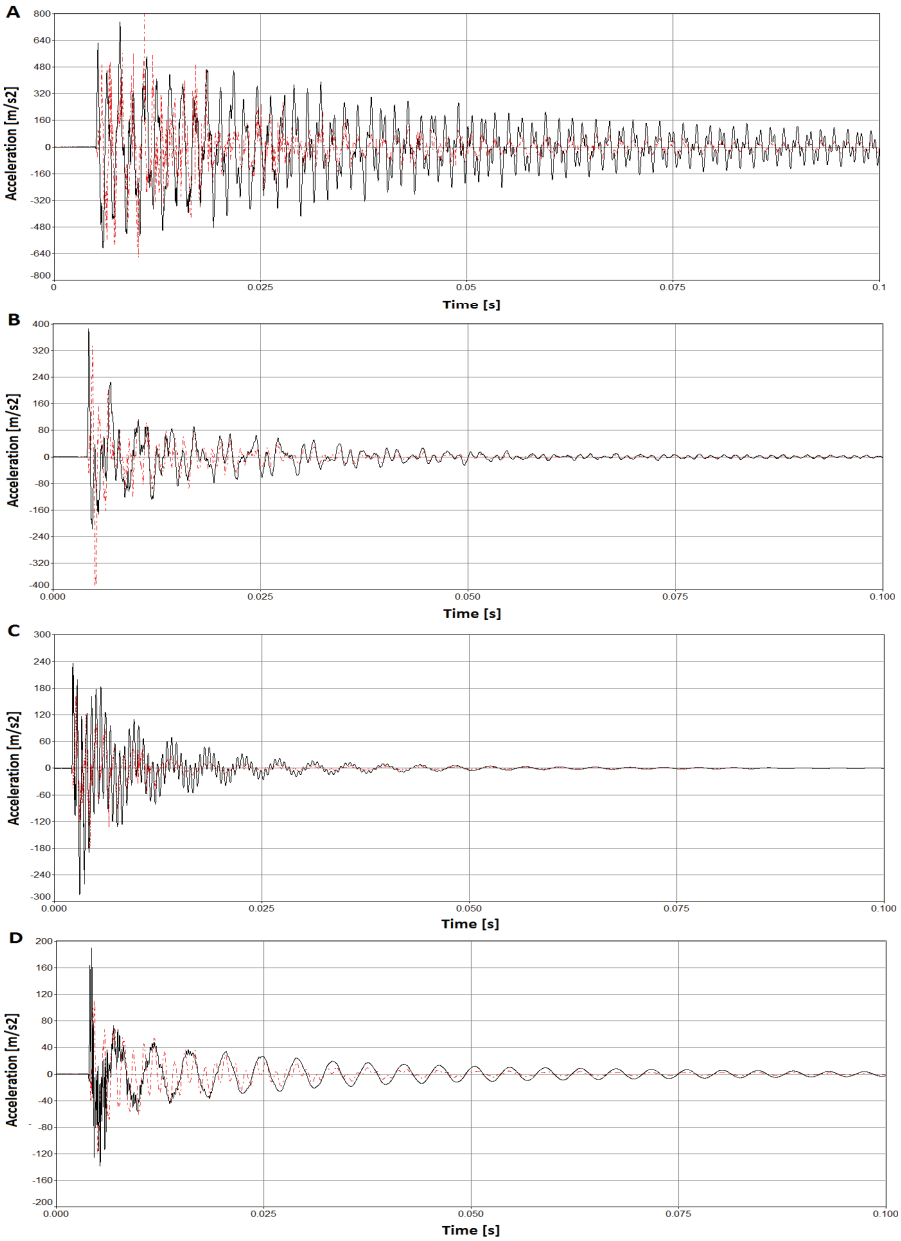

Fig 6. Measured acceleration values in the x direction (solid line: accelerometer 1, dash dot line: accelerometer 2)

Note that the vertical axis of the FFT plot in Fig. 7 does not cover the entire range of natural frequencies; for clearer observation of the lower modes, the entire spectra of the sensors are not illustrated. Based on Fig. 7, it can also be clearly observed that not only the number of peaks in the observed interval is decreasing with the increasing concrete layer but also the peak positions are changing. For each concrete level, the measurements are repeated with the same excitation to eliminate the possible occurrence of extraneous data, and the peaks that remain stable are considered to be the natural modal frequencies of the system belonging to the particular case. The decreasing number of natural frequency modes can be observed in the FFT spectrum as the concrete layer becomes thicker. The change in the rigidity of the structure can also be clearly observed in Fig. 7.

The characteristic vibration parameter values are summarized in Table 3 as the averages of the measurements values for the same excitation type. The table indicates that the decreasing values of these parameters accurately characterize the thickness of the formed concrete layer. As a result of FEM simulations, the gathered natural frequencies of the first three longitudinal type normal modes are illustrated in Fig. 8, and the frequencies values are summarized in Table 4.

The first modes of longitudinal vibration obtained from the FEM can be clearly identified in the measured values. In every case, the first peaks, with one of the highest amplitudes in the FFT spectrum (Fig. 7), are close to the FEM calculation results of the first mode of the natural frequency. The difference may arise from the simplifications of the model, especially in the case of different concrete levels, due to the data of the concrete layer's thickness and mechanical properties. The natural frequencies can also be calculated by the formerly introduced Eq. 1. For the calculation, correction factors must be used: beside the λ frequency factor, which depends on the piping configuration and mode number, a natural frequency correction factor for piping end conditions is also necessary.

The application of this calculation method with the correction factors normally provides answers that are within 15% of the measured frequency values (Wachel et al., 1990). Table 5 presents the first modes of the longitudinal natural frequencies based on the measurements, the finite element method, and the calculated value of the λ frequency factor.

Note that the natural frequency correction factor for piping end conditions is considered to be 0.7 based on Wachel et al. (1990). This correction factor makes the λ value for the first longitudinal natural frequency to be between the simply supported (9.87) and the fixed-fixed (22.4) piping configuration's factor values. This result corresponds to the preliminary expectations, considering the special layout of the experimental system. With the increase of the concrete thickness or the mode number, the frequencies of the circumferential vibration of the piping shell wall significantly shift to higher frequencies.

These frequencies can be calculated by Eq. 2 and only in the case where the initial state has the i=2 mode close to the first mode of the longitudinal frequencies. Thus, the value of shell wall natural resonant frequency at mode i=2 is approximately 688 Hz, which corresponds to 725 Hz calculated by the FEM. Given the previously mentioned 15 percent accuracy, this is also sufficiently accurate.

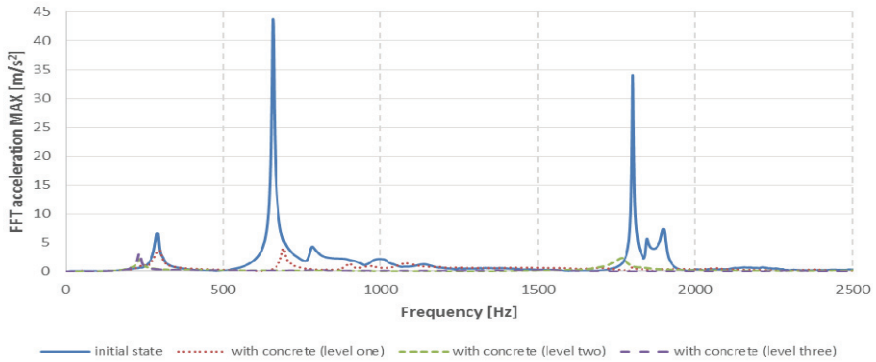

Fig. 7. The frequency spectrum of the middle accelerometer (acc. 1) in the vertical (x) direction

Table 3. Characteristic vibration parameter values, averages for the same vibration excitation (accelerometer 1, x direction)

		a_{peak} [m/s^2]	v_{peak} [mm/s]	d_{peak} [μm]
Initial state	**average value**	**674.53**	**168.34**	**77.41**
	standard dev.	*77.58*	*18.24*	*14.36*
With concrete (level 1)	**average value**	**226.08**	**63.53**	**42.16**
	standard dev.	*35.41*	*7.74*	*6.54*
With concrete (level 2)	**average value**	**115.77**	**45.26**	**30.07**
	standard dev.	*6.42*	*1.66*	*0.67*
With concrete (level 3)	**average value**	**84.44**	**38.80**	**27.31**
	standard dev.	*4.32*	*2.46*	*1.67*

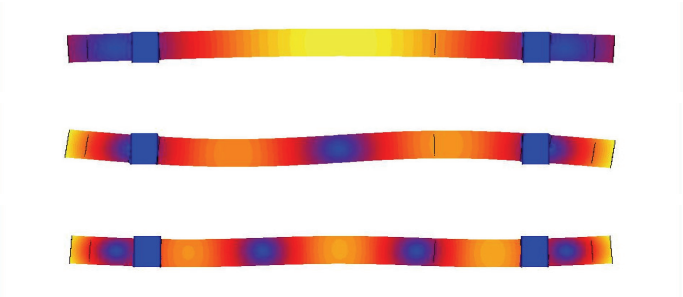

Fig. 8. First three normal modes of the longitudinal vibration (by FEM)

Table 4. The three lowest longitudinal natural frequencies of the system in the case of different amounts of concrete (calculated by FEM)

	Initial state	***With concrete (level one)***	***With concrete (level two)***	***With concrete (level three)***
First mode [Hz]	298	249	231	223
Second mode [Hz]	923	852	799	785
Third mode [Hz]	1713	1579	1497	1478

Table 5. Values of the first natural frequency of the longitudinal vibration and the λ correction factor

	Initial state	***With concrete (level one)***	***With concrete (level two)***	***With concrete (level three)***
Measured value [Hz]	291	247	236	234
FEM value [Hz]	298	249	231	223
λ values with 0.7 end correction factor	10.81	17.44	17.61	17.82

5. Conclusions

Limescale buildup on pipes changes the vibration parameters similar to the experimentally formed concrete layers, for which the changes can be detected by vibration measurements. Such measurements provide information regarding the pipe's status and the thickness of the formed layer in a nondestructive way.

The natural frequency values obtained by the measurement were compared to the results of the finite element simulation. The changes of natural frequencies and the vibration parameter values for a particular type of excitation accurately characterize the pipe's status. This method is also suitable for in situ tests, which is the basis of future measurements.

Acknowledgments

The work/publication is supported by the TÁMOP-4.2.2.A-11/1/KONV-2012-0041 project. The project is co-financed by the European Union and the European Social Fund.

The author acknowledges the Department of Mechanical Engineering of the University of Debrecen, and in particular, István Székács for his indispensable help in the realization of the experiments.

References

Bajcar T., Cimerman F., Sirok B., Amersek M., (2012), Impact assessment of traffic-induced vibration on natural gas transmission pipeline, *Journal of Loss Prevention in the Process Industries*, **25**, 1055-1068.

Drozyner P., (2011), Determining the limits of piping vibration, *Scientific Problems of Machines Operation and Maintenance*, **165**, 97-103.

Hosoya N., Kajiwara I., Hosokawa T., (2012), Vibration testing based on impulse response excited by pulsed-laser ablation: Measurement of frequency response function with detection-free input, *Journal of Sound and Vibration*, **331**, 1355-1365.

Kajiwara I., Hosoya N., (2011), Vibration testing based on impulse response excited by laser ablation, *Journal of Sound and Vibration*, **330**, 5045-5057.

Mattheis A., Trobitz M., Kussmaul K., Kerkhof K., Bonn R., Beyer K., (2000), Diagnostics of piping by ambient vibration analysis, *Nuclear Engineering and Design*, **198**, 131-140.

Lee J.-R., Chong S.Y., Jeong H., Kong C.-W., (2011), A time-of-flight mapping method for laser ultrasound guided in a pipe and its application to wall thinning visualization, *NDT&E International*, **44**, 680-691.

Li S.-J., Liu G.-M., Kong W.-T., (2014), Vibration analysis of pipes conveying fluid by transfer matrix method, *Nuclear Engineering and Design*, **266**, 78-88.

Liu J.X., Li T.Y., Liu T.G., Yan J., (2005), Vibration characteristic analysis of buried pipes using the wave propagation approach, *Applied Acoustics*, **66**, 353-364.

Racasan A., Munteanu C., Topa V., Purcar M., Grindei L., (2011), Computation of the potential induced on the fluid transport pipelines by overhead high voltage lines, *Enivronmental Engineering and Management Journal*, **10**, 505-510

Raggio L.I., Etcheverry J., Sánchez G., Bonadeo N., (2010), Error analysis of the impulse excitation of vibration measurement of acoustic velocities in steel samples, *Physics Procedia*, **3**, 297-303.

Saeed R.A., Galybin A.N., Popov V., (2013), 3D fluid–structure modelling and vibration analysis for fault diagnosis of Francis turbine using multiple ANN and multiple ANFIS, *Mechanical Systems and Signal Processing*, **34**, 259-276.

Semke W.H., Bibel G.D., Jerath S., Gurav S.B., Webster A.L., (2006), Efficient dynamic structural response modelling of bolted flange piping systems, *International Journal of Pressure Vessels and Piping*, **83**, 767-776.

Wachel J.C., Morton S.J., Atkins K.E., (1990), *Piping Vibration Analysis*, Proce. of 19th Turbomachinery Symposium, 119-134, On line at: http://www.engdyn.com/piping/vibration/analysis/url/.

Wang X.H., Redekop D., (2011), Natural frequencies analysis of moderately-thick and thick toroidal shells, *Procedia Engineering*, **14**, 636-640.